ChemElectroChem

Research Article
doi.org/10.1002/celc.202500342

Chemistry Europe
European Chemical Societies Publishing

www.chemelectrochem.org

Theoretical Calculation of Finite-Temperature X-Ray Absorption Fine Structure: Application to Sodium K-Edge in NaCl

Philipp Hönicke, Yves Kayser, and Pouya Partovi-Azar*

This study presents a comprehensive computational framework for reproducing the full X-ray absorption fine structure (XAFS) through quantum-chemical simulations. The near-edge region is accurately captured using an efficient implementation of time-dependent density-functional perturbation theory applied to core excitations, while *ab initio* molecular dynamics provides essential sampling of core-excitation energies and interatomic distance distributions for interpreting extended X-ray absorption fine structure (EXAFS) features. Owing to the efficiency of the approach, the total spectrum can be decomposed into contributions from bulk, defective, and surface environments, which commonly coexist in experimental systems. The methodology is demonstrated for sodium at the Na K-edge in NaCl, where the predicted spectra show good agreement with experimental measurements on thin-film samples. This strategy offers a practical route to generating chemically specific XAFS cross-section data for elements and species that remain challenging to characterize experimentally, thereby enabling deeper insights into materials of technological importance.

1. Introduction

Materials characterization plays a central role in modern science and technology, as it provides the fundamental understanding of structure-property relationships that drive innovation. By probing materials at the atomic, molecular, and macroscopic levels, characterization techniques reveal the chemical composition, electronic structure, and physical properties essential for tailoring performance.[1] From energy storage and catalysis to nanotechnology and biomedical applications, reliable characterization not only accelerates the discovery of new materials but also ensures their functionality, stability, and scalability in real-world technologies.

Experimental characterization techniques, particularly spectroscopic methods, are indispensable for unveiling the microscopic properties of materials. Spectroscopy provides direct insight into vibrational, electronic, and structural features, enabling researchers to probe bonding environments, defect states, and dynamic processes with high precision. Techniques such as infrared, Raman, UV-Vis, and X-ray spectroscopy bridge the gap between fundamental theory and practical application, offering powerful tools to monitor material behavior under operating conditions and to guide the design of next-generation functional materials.[2,3]

In particular, X-ray spectroscopies provide powerful insights into the electronic and structural properties of materials, making them especially valuable for the study of energy-related systems. Techniques such as X-ray absorption fine structure (XAFS) spectroscopy, which includes X-ray absorption near edge spectroscopy (XANES) and extended X-ray absorption fine structure (EXAFS) spectroscopy, and X-ray photoelectron spectroscopy (XPS) allow for a reliable probing of oxidation states, local coordination environments, and electronic structures with element-specific sensitivity.[4–9] This enables a detailed understanding of catalytic activity, charge transport, and chemical transformations in batteries, solar cells, and other energy technologies.[10–16] By capturing both static and dynamic information, X-ray spectroscopies help unravel the mechanisms that govern material performance and stability under realistic operating conditions. Recent works underscore how XAS has become a powerful probe for energy materials under realistic operating conditions. For a recent review on the application of XAFS across Li-ion, Na-ion, and Li–S batteries, see Ref. [15] and the references therein.

With the rise of sodium-based batteries as alternative to lithium-based system, many X-ray spectroscopy studies have

P. Hönicke
Helmholtz-Zentrum Berlin (HZB)
Hahn-Meitner-Platz 1, 14109 Berlin, Germany

P. Hönicke
Physikalisch-Technische Bundesanstalt (PTB)
Abbestr. 2–12, 10587 Berlin, Germany

Y. Kayser
Max Planck Institute for Chemical Energy Conversion
Stiftstr. 34–36, 45470 Mülheim an der Ruhr, Germany

P. Partovi-Azar
Institute of Chemistry
Martin Luther University Halle-Wittenberg
Von-Danckelmann-Platz 4, 06120 Halle (Saale), Germany
E-mail: pouya.partovi-azar@chemie.uni-halle.de

Supporting information for this article is available on the WWW under https://doi.org/10.1002/celc.202500342

© 2025 The Author(s). ChemElectroChem published by Wiley-VCH GmbH. This is an open access article under the terms of the Creative Commons Attribution License, which permits use, distribution and reproduction in any medium, provided the original work is properly cited.

© 2025 The Author(s). ChemElectroChem published by Wiley-VCH GmbH

been carried out to characterize different components of these batteries and decipher mechanisms of the underlying processes during battery operation.[17–22] Correct analysis and quantitative interpretation of X-ray spectroscopies require accurate key atomic fundamental parameters of sodium as well as reliable reference XAFS spectra for relevant sodium chemical species. However, the current knowledge on the fundamental parameters for sodium is limited to outdated data often derived from interpolations of neighboring elements, relying solely on theoretical calculations without experimental validation, and usually suffering from unknown or only estimated uncertainties.

Theoretical calculations of X-ray spectroscopies provide a crucial framework for interpreting and complementing experimental measurements. By simulating core-level excitations and electronic transitions with atomistic accuracy, theory helps disentangle overlapping spectral features and assign them to specific local environments, oxidation states, or bonding motifs.[23–27] Such calculations bridge the gap between raw experimental spectra and the underlying microscopic processes, enabling a more reliable identification of structure–property relationships. In energy-related materials, this combined approach is particularly powerful for tracking redox mechanisms, defect states, and degradation pathways, thereby guiding the rational design of more efficient and durable technologies.[28–31] In fact, theoretical calculations may even be required to determine reference XAFS spectra for relevant but chemically highly sensitive species for which isolated experimental data within operando XAFS datasets of batteries is hard or impossible to be obtained.[32]

In this work, we present practical steps toward theoretical calculation of the compound-specific fine structure components, which allows for the interpretation of experimental XANES and EXAFS data by combining quantum-chemical calculation of core-excitation energies and amplitudes together with ab initio molecular dynamics simulations at finite temperatures. As a target system, we concentrate on the Na K-edge in NaCl in order to assess and benchmark the computations against experimental data. The presented computational procedure will enable us to eventually find the missing chemically specific cross-section data in existing fundamental parameters tabulations for sodium as well as for sodium species, which are relevant for Na-ion based battery materials but very hard to be addressed experimentally because of high chemical sensitivity or instability.

2. Methodology

The theoretical investigation have been performed for three systems, namely a perfect NaCl crystal, a defective NaCl crystal, both using a 11.176Å × 11.176Å × 11.176Å unit cell, and a NaCl (100) surface using a 22.000Å × 11.176Å × 11.176Å unit cell (**Figure 1**). The unit cells for the perfect crystal and (100) surface contained 64 atoms, whereas two chlorine atoms were removed from the one considered for the defective sample. Periodic boundary conditions were used for all calculations.

Finite-temperature effects have been included by performing *ab initio* molecular dynamics (AIMD) simulations at two different

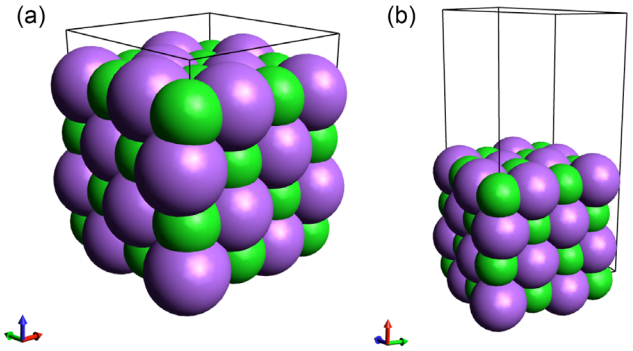

Figure 1. AIMD snapshots of the structures representing a) NaCl bulk structure and b) NaCl (100) surface together with their respective unit cells considered here. Purple and green spheres denote chlorine and sodium ions, respectively.

temperatures, namely $T = 300$ K and $T = 400$ K, using the CP2K software package.[33] The AIMD simulations have been performed at electronic ground state and serve to provide a set of snapshots for every system at a finite temperature to be further used for XANES simulations. For each system, an AIMD simulation has been first carried out in the canonical ensemble for 20 ps using CSVR thermostat.[34] A time step of 1 fs was chosen for atomic coordinate propagation. The atomic forces for integrating the equation of motion during AIMD have been calculated at density-functional theory (DFT) level,[35,36] where the core electrons have been effectively taken into account via Goedecker–Tetter–Hutter-type pseudopotentials,[37–39] while the valence electrons have been described using the mixed Gaussian and plane wave basis set DZVP-MOLOPT-SR.[40] Exchange and correlation effects have been approximated using the PBE functional[41,42] together with the semi-empirical DFT-D3 method[43] to correct for the long-range dispersion interactions. A plane-wave energy cutoff of 500 Ry and a relative cutoff of 50 Ry were chosen. After the equilibration phase, the atomic coordinates have been sampled in the micro canonical ensemble for an additional 20 ps. A similar procedure involving AIMD simulations has been already adopted before for ab initio simulation of finite-temperature vibrational spectra.[44–47] To simulate the XANES, these trajectories have been used afterwards to calculate core-excitation energies and corresponding excitation amplitudes.

There have already been valuable strides toward theoretical calculation of XANES based on quantum-chemical methods, such as ΔSCF,[48] transition-potential DFT,[49–51] real-time[52] and linear-response time-dependent DFT (TDDFT),[53–55] and wavefunction-based methods.[56,57] Wavefunction based methods give by far the most accurate results with an excellent agreement with experimentally measured XANES spectra. However, their huge computational cost limits their use to small molecular systems.[23] Here, the core excitations have been studied using time-dependent density-functional perturbation theory (TDDFPT) within Tamm–Dancoff approximation.[58] To calculate the core excitations, we have assumed that the core and valence states only weakly couple, due to the large difference in their energies. Following the work of Bussy and Hutter,[59] we have also assumed that the

© 2025 The Author(s). ChemElectroChem published by Wiley-VCH GmbH

relaxation of electrons beyond the core region is negligible upon excitation of a core electron. In a simplified picture, fast relaxations of the valence electrons due to an effectively positive charge in the core region (that of the core hole after the excitation of an electron) result in lowering of the energy of the final electronic configuration. Therefore, ignoring such relaxations could result in an overestimation of core-excited energies. Adopting the above approximations, all required 4-center 2-electron integrals involve the excited core state (here sodium 1*s*) and, therefore, allows for a core-specific resolution of the identity scheme.[59] A PBEh ($\alpha = 0.45$)[60] hybrid exchange-correlation functional has been used. All-electron basis set aug-pcseg-2[61] has been employed only for one Na atom in the structures while other atoms have been treated within the pseudopotential formalism to reduce the computational cost. Periodic Hartree–Fock calculations have been performed for all systems using the truncated coulomb potential[62] together with the auxiliary density matrix method and corresponding basis set aug-admm-2[63] only on the excited Na atom, where core excitations from 1*s* level have been investigated. The core-excitation energies and oscillator strengths have been computed on reference trajectories described above and sampled every 10 fs. TDDFPT calculations have also been performed using CP2K software. The excitation energies from core levels obtained from TDDFPT calculations should normally be shifted to match the experiments. This is related to the well-known self-interaction error in DFT calculations as well as to the lack of orbital relaxation upon the creation of the core hole in TDDFPT scheme adopted here. However, this can be substantially corrected for using the ab initio correction method GW2X*.[64,65] It has been shown that using PBEh XC functional together with the GW2X* method could lead to computed resonance energies in good agreement with experiments.[65]

For comparison purposes, a NaCl thin-film coating on a silicon nitride (SiN) membrane is used. The NaCl coating has a nominal mass deposition of (102.5 ± 5.2) μg cm^{-2}, corresponding to a thickness of about 470 nm using the tabulated bulk density of NaCl, while the carrier membrane has a nominal thickness of 1000 nm. Both the XANES and the EXAFS of this sample at the Na K-edge have been measured in transmission mode employing the plane grating monochromator beamline of the Physikalisch–Technische Bundesanstalt at BESSYII.[66] For reference purposes and for subtraction of the carrier membrane contribution, also a blank membrane of nominally identical thickness was used. These experiments have been carried out using an in-house developed ultra-high vacuum chamber,[67] which is equipped with calibrated photo diodes used to determine and monitor the incident photon flux at each probed monochromatic photon energy. The samples were aligned to be in the center of the experimental chamber by an *x*-*y*-scanning stage. For all experiments, both the sample orientation with respect to the synchrotron radiation beam was 45°. For the transmission experiments, the incident photon energy was varied from 990 eV to 1300 eV in small steps (0.2 eV) in the vicinity of the sodium K attenuation edge and in larger steps (1 eV) below and further away from this edge. For each incident photon energy, 10 readings of a photo diode placed in the beam behind the sample were recorded and averaged. Further details can be found in Ref. [68].

From the transmission data, the sample specific mass attenuation coefficients (product of the mass attenuation coefficient μ, material density ρ, and thickness d) can be derived employing the Beer–Lambert law. In the case of the NaCl on SiN, it represents the sum of the sample specific mass attenuation of NaCl and SiN, respectively. Using the transmission data from the blank SiN membrane, the contribution for NaCl can then be isolated and the sample specific mass attenuation factors $\mu_{S,NaCl}(E_0)\rho d$ for NaCl can be obtained. The contribution from the Na K-shell was isolated by scaling the relevant partial subshell contributions using Ebel polynomials[69] into the $\mu_{S,NaCl}(E_0)\rho d$ dataset. As the relative contributions for the coherent and incoherent scattering are low in this photon energy regime, the isolated Na K-shell contribution is the sample specific photoionization cross section $\tau_{\mathrm{Tot,NaCl}}(E_0)\rho d$.

The XAFS spectra were analyzed using the Xraylarch software package.[70] The E_0 value (ionization threshold) was determined using the maximum in the derivative of the XAFS spectrum. First- and second-order pre- and post-edge polynomials were used to produce a normalized spectrum. The autobk algorithm included in Larch was then used to calculate the $\chi(k)$, the EXAFS structure in *k*-space. The k^2-weighted EXAFS data were then Fourier-transformed to *r*-space using an FFT, with a Hanning window ranging from 2 Å^{-1} to 10 Å^{-1} with an edge width of 10 Å^{-1} being applied.

3. Results and Discussion

The calculated XANES of the above systems are presented in **Figure 2**a. These calculations have been performed with the computational setup described above using the PBEh functional. For a comparison with the spectra calculated using the PBE0 functional, please see the Supporting Information. As seen in the lower panel, the elevated temperature results in broader peaks and overall smoother, less-featured spectrum. It should be emphasized again that here the effect of finite temperature on the spectrum has been included only through computation of oscillator strengths for core excitations averaged over an AIMD trajectory obtained at the electronic ground state. A pre-edge activity is also seen in the XANES of the perfect crystals at both temperatures. Main features above 1090 eV are also observed in the defective bulk system (blue). Although the photon energies corresponding to the resonances close to the threshold (1080–1085 eV) are also seen in the defective system, but their relative intensities differ significantly. Additionally, a small peak is observed at lower energies in the XANES of the defective sample, ≈1.5 eV lower than the pre-edge peak in the perfect system. Analyzing the projected density of states reveals that (see the Supporting Information) this peak, unlike the weak pre-edge peak in the bulk NaCl, can be assigned to an excitation from the 1*s* state to the 3*p* state of the excited Na atom. The analysis also

© 2025 The Author(s). ChemElectroChem published by Wiley-VCH GmbH

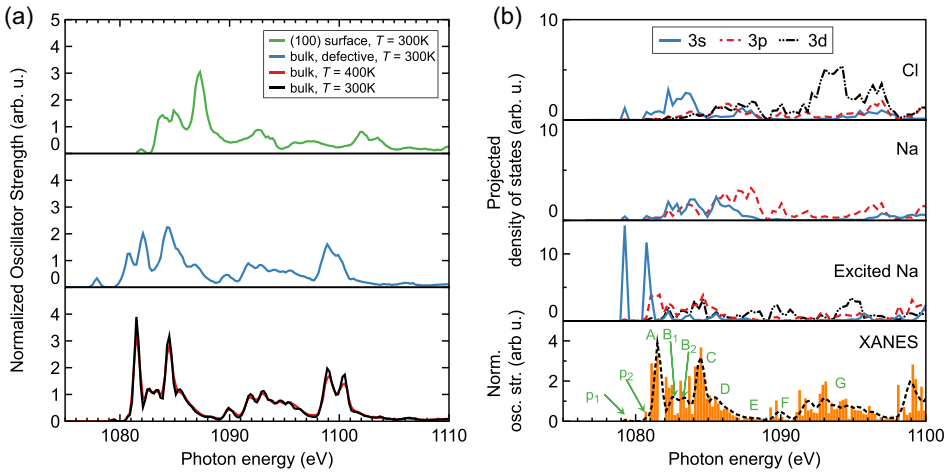

Figure 2. a) Computed XANES of the perfect NaCl crystal at $T = 300$ K (black) and $T = 400$ K (red), as well as that of the defective sample (blue) and the aCl (100) surface (green), both at $T = 300$ K. b) Upper three panels: Projected density of states (PDOS) onto the individual Na and Cl states in the near-edge region of the perfect NaCl sample; 3*s*: blue, 3*p*: red, 3*d*: black. Lower panel shows the calculated XANES of a single AIMD snapshot of the perfect NaCl bulk sample (orange), and an averaged spectrum computed over the entire AIMD trajectory at $T = 300$ K (dashed black).

shows that the dipole-forbidden transition to 3*s* state of the excited atom in the defective bulk system almost coincides in energy with the pre-edge peak in the bulk NaCl and only results in an unnoticeable shoulder at ≈1080 eV in the XANES of the defective sample. For a detailed analysis, see the discussion below as well as the Supporting Information. The spectrum for the (100) surface exhibits substantial differences as compared to the spectra of the perfect and defective bulk systems. Apart from the resonances in 1080–1082 eV range becoming considerably insignificant, a strong peak is observed at around 1087 eV and a broader one above 1100 eV. The blueshift observed in the position of the first resonance in the case of (100) surface can partially be related to a more strongly bound 1*s* electron of the excited Na atom on the surface (see the Supporting Information).

Figure 2b shows the calculated XANES for a single AIMD snapshot of the bulk NaCl system (orange bars, lower panel). For comparison, the XANES obtained as an average over the individual spectra of AIMD snapshots at $T = 300$ K is shown in dashed black. The significant differences between the orange bars and dashed black curve emphasizes the importance of finite-temperature effects in reliable calculation of X-ray spectroscopies. The above three panels in Figure 2b show the projected density of states (PDOS) in the near-edge region for the absorber (excited) Na atom, as well as the remaining Na and Cl atoms. In agreement with previously reported DFT studies,[71] the PDOS analysis reveals that the two observed pre-edge peaks, p_1 and p_2, mainly arise from an $1s \rightarrow 3s$ transition in the excited Na atom, only allowed through the much weaker quadrupole mechanism in geometries differing from perfect crystal, such as those at finite temperatures. The 3*s* states of chlorine and other sodium atoms could also contribute, to a much smaller degree, to the observed pre-edge peaks (see two upper panels in Figure 2b). The main peak A can be solely attributed to $1s \rightarrow 3p$ transition in the excited Na. The peaks B_1 and B_2 can be mainly assigned again to excitations from 1*s*–3*p* in all Na species. There are also some small overlaps from 3*s* states of Cl and Na, as well as that of the excited Na 3*d*, observed around these two peaks, all of which should be dipole forbidden. Similarly, peak C should also arise from an excitation to Na 3*p* states which have an overlap with Cl 3*s* states.[71] Finally, while peak D can be attributed to excitations from the 1*s* state of the excited Na atom to the 3*p* states of all Na atoms, peaks E and F can be assigned to transitions mainly to Na 3*p* and partially to those of Cl. Around peaks E and F, there are also contributions observed from the excited Na and Cl 3*d* states, which should only be weak due to dipole selection rule. The broad peak G can generally be attributed to excitations to the 3*d* states of sodium and chlorine atoms, weakly allowed due to thermal atomic fluctuations.

In order to incorporate the effects from different structures to an X-ray near-edge spectrum comparable to an experimental XAFS spectrum of a thin-film sample (which presumably encompasses perfect and defective NaCl crystallites as well as different crystal surfaces), we have computed a "total" spectrum as a linear combination of the individual spectra presented in Figure 2a. **Figure 3** shows the calculated XANES for the perfect NaCl crystal (orange), defective crystal (green), and NaCl (100) surface (red), as well as the experimental XANES measured for a NaCl thin-film sample (blue). Also shown in Figure 3 is a linear combination of computed spectra, with manually selected weights (purple, 63% of the perfect NaCl crystal, 26% of the defective crystal, and 11% of the NaCl (100) surface). It should be noted that since the ionizations into the continuum at higher photon energies are not fully incorporated in the TDDFPT calculations here, a more systematic fit to the experimental data is not yet feasible. All the computed spectra have been rigidly shifted about 5 eV in energy to match the energy corresponding to the first experimentally observed resonance. Without the GW2X* correction scheme, this difference has been observed to be around 22 eV, which was also reported for other systems.[65] As stated

© 2025 The Author(s). ChemElectroChem published by Wiley-VCH GmbH

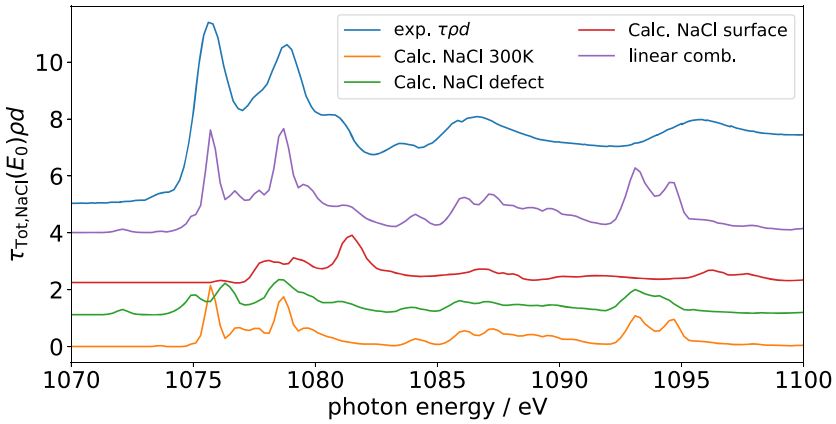

Figure 3. Calculated XANES for the perfect aCl crystal (orange), defective crystal (green), and naCl (100) surface (red). Experimental spectrum measured for a thin-film sample is also shown (blue). Purple curve represents a linear combination of the computed spectra with different weights (purple, 63% of the perfect NaCl crystal, 26% of the defective crystal and 11% of the NaCl (100) surface). The spectra were shifted vertically for clarity.

earlier, the observed discrepancy can be related to the self-interaction error in the DFT calculations and the lack of orbital relaxation upon the creation of the core hole.[65] The relative intensities and peak positions are well reproduced by the purple spectrum. The agreement between the theory and experiment is remarkable up to 1090 eV. The discrepancy between the purple and blue curves becomes more profound at around and above 1095 eV, which might be an indicator that the contribution of the NaCl surfaces (red) to the overall spectrum could be more substantial. However, it should be noted that the actual crystal structure of the NaCl thin film on the SiN carrier membrane is likely to be more complex.

The calculated radial distribution functions, $g(r)$, are shown on upper panels of **Figure 4**, while the lower panels show the number of neighbors of typical Na reference atom. While the radial distribution functions and the number of neighboring atoms in the perfect (both at $T = 300$ K and $T = 400$ K) and defective samples slightly differ from one another, the most profound difference is observed in the case of NaCl (100) surface. The nearest neighbor distance from a reference Na atom (Cl) in all the systems is found to be around 2.75 Å, while the second nearest neighbor (Na) is found at about 3.95 Å. The thirst nearest neighbor (Cl) is slightly shifted from 4.85Å in the perfect and defective samples to ≈4.95Å. in the case of (100) surface.

The EXAFS data together with the applied Hanning window is shown in **Figure 5**a, while the magnitude of the non-phase-shift-corrected FFT obtained from the experimental EXAFS data in r-space is shown in Figure 5b in light gray. The black curve in Figure 5b is a scaled radial distribution function, $g_{Na-all}(r)$ obtained from the AIMD simulations on the defective crystal system (blue curve in the upper-right panel of Figure 4). The discrepancy between the experimental data (dashed light

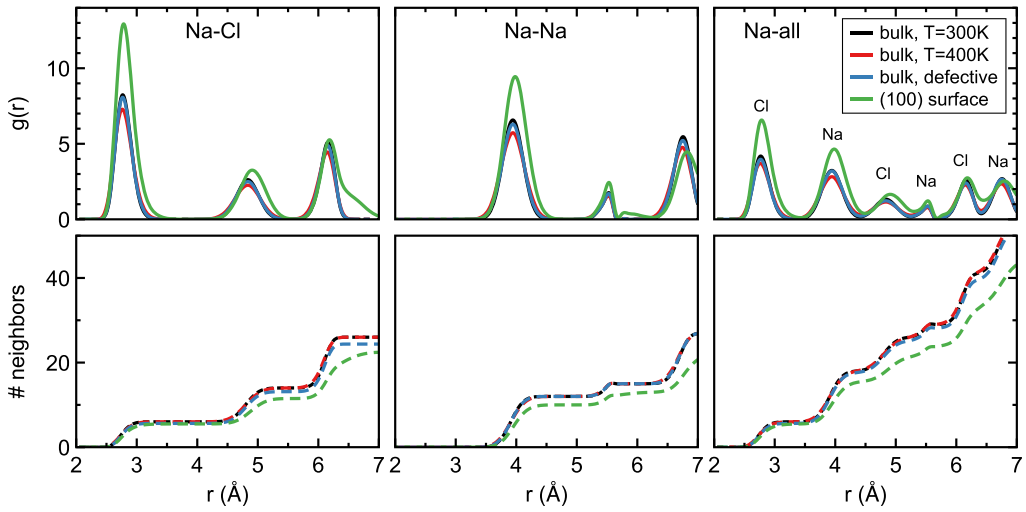

Figure 4. Radial distribution functions (upper panels) of Na-Cl (left), Na–Na (middle), and a-all (right) in different systems, namely perfect crystal at $T = 300$ K (black), perfect crystal at $T = 400$ K (red), defective crystal (blue), and naCl (100) surface (green). Please note the different normalization factors for $g(r)$ in each system. The panels on the lower row show the corresponding number of neighboring atoms from a typical sodium atom.

© 2025 The Author(s). ChemElectroChem published by Wiley-VCH GmbH

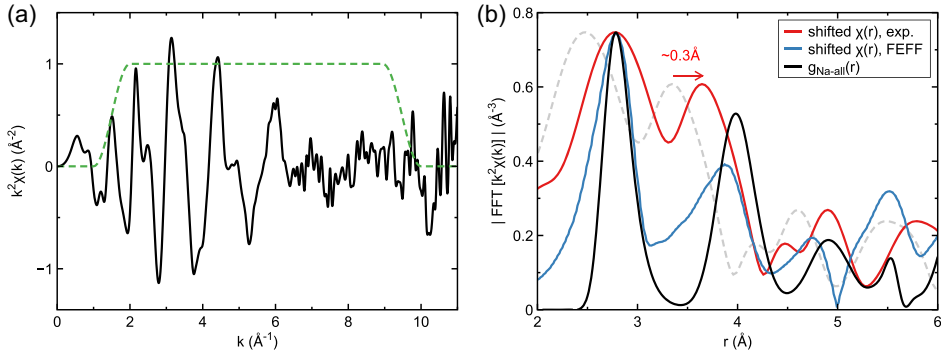

Figure 5. a) EXAFS data (black) together with used Hanning windows (green). b) Magnitude of the non-phase-shift-corrected FFT of the EXAFS data (light gray) together with the same FFT data rigidly shifted by ≈0.3 Å (red). Also shown in black is a scaled radial distribution function, $g_{Na-all}(r)$ obtained from the AIMD simulations on the defective crystal system (Figure 4). For a better comparison, the rigid shift and the scaling factor were chosen so that the first peaks in the red and black curve coincide in both position and intensity.

gray) and the calculated radial distribution function (solid black) is due to a phase-shift in the scattering process, which necessitates a rigid shift in energy applied to the experimental data. The same FFT data with a rigid shift of ≈0.3 Å is shown in red. For a better comparison, the rigid shift and the scaling factor were chosen so that the first peaks in the red and blacks curve coincide in both position and intensity. Although the agreement between the experimental and theoretical results seems acceptable, the main difference appears to occur at around 3.65 Å and about 4.50 Å. This could be related to the considerable structural difference of thin film samples used in the measurements and relatively simple system considered in the computations. Additionally, the discrepancy at above 5 Å could be related to relatively small unit cell size in the calculations. The agreement with the experimental EXAFS at around this distance can be slightly improved using bigger super cells (please see the Supporting Information). Moreover, we have performed a FEFF calculation using scattering paths generated by FEFF8L as incorporated in the Xraylarch program,[70] starting from a $2 \times 2 \times 2$ cell for bulk NaCl that was replicated into a $3 \times 3 \times 3$ cell in order to allow for calculations over a larger *r*-range for capturing more scattering paths and reducing edge effects. The calculation was performed without including a Debye–Waller factor, but including a fixed sigma_square factor of 0.005, a value that is within the commonly recommended range for ionic systems. These factors impact peak heights and shapes but were not further optimized since the intended goal was to confirm the positions from Na and Cl scatterers (with Na being the absorber). Hence, no fitting was attempted, where optimization of further parameters would be required and cross-correlations need to be considered. As discussed, the first-shell peak (6 Cl scatterers) appears lower than the true distance due to the phase shift, but the shift between calculated and experimental data is identical. Hence, the required qualitative shift (0.3 Å) to match the radial distribution function from the AIMD simulations can be considered, as it is validated by the FEFF calculations. The second-shell peak (12 Na scatterers) shows a slightly different phase shift, but is still in qualitative agreement with $g_{Na-all}(r)$, with less than 0.1Å difference.

4. Conclusions

In this work, we have shown that the complete X-ray absorption fine structure (XAFS) can be reliably reproduced using state-of-the-art quantum-chemical methods. The near-edge spectral features are accurately described through an efficient implementation of time-dependent density-functional perturbation theory applied to core electrons, while *ab initio* molecular dynamics simulations prove essential both for sampling core-excitation energies and for providing radial distribution functions that enable a direct interpretation of the extended X-ray absorption fine structure (EXAFS). The combined approach has been successfully applied to the Na K-edge in NaCl, yielding theoretical spectra in good agreement with experimental measurements on thin-film samples. Thanks to the efficiency of the employed methodology, we were further able to disentangle the spectral contributions originating from bulk crystals, lattice defects, and surfaces-structural motifs that are typically present in experimentally studied samples. Altogether, this computational framework provides a robust pathway for generating chemically specific XAFS cross sections of elements and compounds that remain difficult or even impossible to characterize experimentally.

Acknowledgements

P.P.-A. gratefully acknowledges DFG funding via projects 420536636 and 446879138, as well as the computing time made available on the high-performance computer at the NHR Center of TU Dresden via the project “p_oligothiophenes”. Y.K. thanks the Max Planck Society for funding. In addition, the work was partially supported by the project 14ACMOS (grant agreement number 101096772), which is funded by the Chips Joint Undertaking and its members, including the top-up funding of Belgium and the Netherlands. Parts of this research have been supported by Hi-Acts, an innovation platform under the grant of the Helmholtz Association HGF within the project BATIX.

Open Access funding enabled and organized by Projekt DEAL.

© 2025 The Author(s). ChemElectroChem published by Wiley-VCH GmbH

Conflict of Interest

The authors declare no conflict of interest.

Author Contributions

Philipp Hönicke: conceptualization, funding acquisition, formal analysis, investigation, methodology, visualization, validation, writing (original draft, review and editing). **Pouya Partovi–Azar**: conceptualization, funding acquisition, formal analysis, investigation, methodology, visualization, validation, writing (original draft, review and editing). **Yves Kayser**: formal analysis, methodology, validation, writing (review and editing).

Data Availability Statement

The data that support the findings of this study are available from the corresponding author upon reasonable request.

Keywords: ab initio molecular dynamics · extended X-ray absorption fine structure · quantum chemistry · time-dependent density functional theory · X-ray absorption fine structure

[1] Y. Leng, *Materials Characterization: Introduction to Microscopic and Spectroscopic Methods*, 2nd Ed., Wiley-VCH Verlag GmbH & Co., Wingheim **2013**.
[2] S. Agnello, *Spectroscopy for Materials Characterization*. 1st Ed., John Wiley and Sons, Inc., NJ, USA **2021**.
[3] D. K. Singh, M. Pradhan, A. Materny, *Modern Techniques of Spectroscopy: Basics, Instrumentation, and Applications*, Springer, Singapore **2021**.
[4] A. Iglesias-Juez, G. L. Chiarello, G. S. Patience, M. O. Guerrero-Pérez, *EXAFS. Canadian J. Chem. Eng.* **2022**, *100*, 3.
[5] A. M. Damjanović, A. T. S. Freiberg, A. Siebel, B. Koyutürk, D. Menga, K. Krempl, P. Madkikar, O. Proux, H. A. Gasteiger, M. Piana, *ChemElectroChem* **2023**, *10*, e202300185.
[6] J. M. Ramallo-López, G. F. Santori, L. Giovanetti, M. L. Casella, O. A. Ferretti, F. G. Requejo, *J. Phys. Chem. B.* **2003**, *107*, 11441.
[7] M. A. Peck, M. A. Langell, *Chem. Mater.* **2012**, *24*, 4483.
[8] M. Anwar, M. A. Shaikh Abdul, U. M. Khan, M. Hassan, A. H. Khoja, A. Muchtar, *Materials* **2022**, *15*, 2540.
[9] A. Zimina, A. Léon, R. Steininger, *Phys. Chem. Chem. Phys.* **2024**, *26*, 2613.
[10] Y. Zubavichus, Y. L. Slovokhotov, M. K. Nazeeruddin, S. Zakeeruddin, M. Grätzel, V. Shklover, *Chem. Mater.* **2002**, *14*, 3556.
[11] M. Babucci, D. M. Meira, E. Wallin, J. Keller, O. Donzel-Gargand, C. Platzer Björkman, N. M. Martin, *Acs Appl. Energy Mater.* **2023**, *6*, 9264.
[12] C. Schwartz, D. Nordlund, T.-C. Weng, D. Sokaras, L. Mansfield, A. S. Krishnapriyan, K. Ramanathan, K. E. Hurst, D. Prendergast, S. T. Christensen, *Solar Energy Mater. Solar Cells* **2016**, *149*, 275.
[13] B. V. Kerr, H. J. King, C. F. Garibello, P. R. Dissanayake, A. N. Simonov, B. Johannessen, D. S. Eldridge, R. K. Hocking, *Energy & Fuels* **2022**, *36*, 2369.
[14] X. Liu, Weng, *Bulletin* **2016**, *41*, 466.
[15] Y. Fan, X. Wang, G. Bo, X. Xu, K. W. See, B. Johannessen, W. K. Pang, *Adv. Sci.* **2025**, *12*, 2414480.
[16] C.-L. Dong, Vayssieres, *Chem.–A Euro. J.* **2018**, *24*, 18356.
[17] A. Brennhagen, A. Skurtveit, D. S. Wragg, C. Cavallo, A. O. Sjastad, A. Y. Koposov, H. Fjellvag, *Chem. Mater.* **2024**, *36*, 7514.
[18] J. Plotek, A. Kulka, A. Maximenko, L. Kondracki, S. Trabesinger, M. Moździerz, P. Czaja, J. Molenda, *Energy Storage Mater.* **2024**, *72*, 103780.
[19] H. Zhang, L. Wang, P. Zuo, *J. Mater. Chem. A.* **2024**, *12*, 30971.
[20] V. Shipitsyn, R. Jayakumar, W. Zuo, B. Sun, L. Ma, *Batteries* **2023**, *9*, 461.
[21] S. Jeong, H. Kang, S. Ryu, G. Oh, Y.-C. Jung, C. Hwang, T.-Y. Yu, J. T. Kim, H.-G. Jung, Y.-K. Sun, et al, *ACS Appl. Mater. & Interfaces* **2024**, *16*, 44737.
[22] Y. Wu, W. Shuang, Y. Wang, F. Chen, S. Tang, X.-L. Wu, Z. Bai, L. Yang, J. Zhang, *Electrochem. Energ. Rev.* **2024**, *7*, 17.
[23] P. Norman, A. S. Dreuw, *Chem. Rev.* **2018**, *118*, 7208.
[24] F. Montorsi, F. Segatta, A. Nenov, S. Mukamel, M. Garavelli, *J. Chem. Theory & Comput.* **2022**, *18*, 1003.
[25] J. Vinson, J. Rehr, J. Kas, E. Shirley, *Phys. Rev. B* **2011**, *83*, 115106.
[26] N. P. Gaba, C. E. de Moura, R. Majumder, A. Y. Sokolov, *Phys. Chem. Chem. Phys.* **2024**, *26*, 15927.
[27] K. Bzheumikhova, J. Vinson, R. Unterumsberger, Y. Kayser, T. Jach, B. Beckhoff, *Phys. Rev. B.* **2022**, *106*, 125133.
[28] F. Weber, J. Ren, T. Petit, A. Bande, *Phys. Chem. Chem. Phys.* **2019**, *21*, 6999.
[29] J. Ren, L. Lin, K. Lieutenant, C. Schulz, D. Wong, T. Gimm, A. Bande, X. Wang, T. Petit, *Small Methods* **2021**, *5*, 2000707.
[30] C. Ortiz-Mahecha, L. Schwob, J. Leroux, S. Bari, R. H. Meißner, A. Bande, *Phys. Chem. Chem. Phys.* **2025**, *27*, 8202.
[31] T. A. Pascal, K. H. Wujcik, J. Velasco-Velez, C. Wu, A. A. Teran, M. Kapilashrami, J. Cabana, J. Guo, M. Salmeron, N. Balsara, et al, *J. Phys. Chem. Lett.* **2014**, *5*, 1547.
[32] C. Zech, P. Hönicke, Y. Kayser, S. Risse, O. Grätz, M. Stamm, B. Beckhoff, *J. Mater. Chem. A.* **2021**, *9*, 10231.
[33] T. D. Kühne, et al, *J. Chem. Phys.* **2020**, *152*, 194103.
[34] G. Bussi, D. Donadio, M. C. Parrinello, *J. Chem. Phys.* **2007**, *126*, 014101.
[35] P. Hohenberg, W. Kohn, *Phys. Rev.* **1964**, *136*, B864.
[36] W. Kohn, L. J. Sham, *Phys. Rev.* **1965**, *140*, A1133.
[37] S. Goedecker, M. Teter, J. Hutter, *Phys. Rev. B.* **1996**, *54*, 1703.
[38] C. Hartwigsen, S. Goedecker, J. Hutter, *Phys. Rev. B.* **1998**, *58*, 3641.
[39] C. Hartwigsen, S. Goedecker, J. Hutter, *Theor. Chem. Acc.* **2005**, *114*, 145.
[40] J. VandeVondele, J. Hutter, *J. Chem. Phys.* **2007**, *127*, 114105.
[41] J. P. Perdew, K. Burke, M. Ernzerhof, *Phys. Rev. Lett.* **1996**, *77*, 3865.
[42] J. P. Perdew, K. Burke, M. Ernzerhof, *Rev. Lett, Phys. Rev. Lett.* **1996**, *77–78*, 1396–1396. 1997.
[43] S. Grimme, J. Antony, S. Ehrlich, H. Krieg, *J. Chem. Phys.* **2010**, *132*, 154104.
[44] R. Kiani, M. Steimecke, M. Alqaisi, M. Bron, D. Sebastiani, P. Partovi-Azar, *Rsc Adv.* **2023**, *13*, 27756.
[45] R. Kiani, H. Sheng, T. Held, O. Löhmann, S. Risse, D. Sebastiani, P. A. Partovi-Azar, *ChemPhysChem* **2025**, *26*, e202400681.
[46] P. Partovi-Azar, *Physical Review B.* **2023**, *108*, 235157.
[47] P. Partovi-Azar, T. D. Kühne, P. Kaghazchi, *Phys. Chem. Chem. Phys.* **2015**, *17*, 22009.
[48] N. A. Besley, A. T. Gilbert, P. M. Gill, *J. Chem. Phys.* **2009**, *130*, 124308.
[49] B. Hetényi, F. De Angelis, P. Giannozzi, R. Car, *J. Chem. Phys.* **2004**, *120*, 8632.
[50] D. Jayawardane, C. J. Pickard, L. Brown, M. Payne, *Phys. Rev. B.* **2001**, *64*, 115107.
[51] D. Hait, M. Head-Gordon, *Highly Accurate Prediction of Core Spectra of Molecules at Density Functional Theory Cost: Attaining Sub-Electronvolt Error from a Restricted Open-Shell Kohn-Sham Approach. the, J. Phys. Chem. Lett.* **2020**, 11, 775–786.
[52] K. Lopata, B. E. Van Kuiken, M. Khalil, N. Govind, *J. Chem. Theory Comput.* **2012**, *8*, 3284.
[53] M. Stener, G. Fronzoni, M. de Simone, *Chem. Phys. Lett.* **2003**, *373*, 115.
[54] N. A. Besley, A. Noble, *J. Phys. Chem. C.* **2007**, *111*, 3333.
[55] S. D. George, T. Petrenko, F. Neese, *Inorganica Chim. Acta* **2008**, *361*, 965.
[56] S. Coriani, H. C. Koch, *J. Chem. Phys.* **2015**, *143*, 181103.
[57] M. L. Vidal, X. Feng, E. Epifanovsky, A. I. Krylov, S. Coriani, *J. Chem. Theory Comput.* **2019**, *15*, 3117.
[58] S. Hirata, M. Head-Gordon, *Chem. Phys. Lett.* **1999**, *314*, 291.
[59] A. Bussy, J. Hutter, *Phys. Chem. Chem. Phys.* **2021**, *23*, 4736.
[60] C. Adamo, V. Barone, *J. Chem. Phys.* **1999**, *110*, 6158.
[61] F. Jensen, *J. Chem. Theory Comput.* **2015**, *11*, 132.
[62] M. Guidon, J. Hutter, J. VandeVondele, *J. Chem. Theory Comput.* **2009**, *5*, 3010.
[63] C. Kumar, H. Fliegl, F. Jensen, A. M. Teale, S. Reine, T. Kjærgaard, *Int. J. Quantum Chem.* **2018**, *118*, e25639.
[64] Y. Shigeta, A. Ferreira, V. Zakrzewski, J. Ortiz, *Int. J. Quantum Chem.* **2001**, *85*, 411.
[65] A. Bussy, J. Hutter, *J. Chem. Phys.* **2021**, *155*, 034108.
[66] F. Senf, U. Flechsig, F. Eggenstein, W. Gudat, R. Klein, H. Rabus, G. Ulm, *J. Synchrotron Rad.* **1998**, *5*, 780.

© 2025 The Author(s). ChemElectroChem published by Wiley-VCH GmbH

[67] J. Lubeck, B. Beckhoff, R. Fliegauf, I. Holfelder, P. Hönicke, M. Müller, B. Pol-lakowski, F. Reinhardt, J. Weser, *Rev. Sci. Instrum.* **2013**, *84*, 045106.
[68] M.-L. Venzke, K. Frenzel, P. Partovi-Azar, P. Hönicke, *Spectrochimica Acta Part B: Atomic Spectro.* **2025**, *233*, 107303.
[69] H. Ebel, R. Svagera, M. Ebel, A. Shaltout, J. Hubbell, *X-Ray Spectrom.* **2003**, *32*, 442.
[70] M. Newville, *J. Phys.: Conference Series* **2013**, *430*, 012007.
[71] G. J. McIntosh, A. Chan, *Phys. Chem. Chem. Phys.* **2018**, *20*, 24033.

Manuscript received: August 30, 2025
Revised manuscript received: October 9, 2025
Version of record online:

© 2025 The Author(s). ChemElectroChem published by Wiley-VCH GmbH